Bastille Day storm: Global response of the terrestrial ring current

P. C:son Brandt (pontus.brandt@jhuapl.edu), D. G. Mitchell and E. C. Roelof
The Johns Hopkins University, Applied Physics Laboratory, Maryland, USA

J. L. Burch
Southwest Research Institute, Texas, USA

Abstract. Global images of the Earth's inner magnetosphere and its response to the coronal mass ejection (CME) on the 15 July, 2000 were obtained by the IMAGE spacecraft. The images were taken in energetic neutral atoms (ENA) by the High Energy Neutral Atom (HENA) imager. ENAs are produced by charge exchange between the hot ion population of the magnetosphere and the cold neutral hydrogen geocorona. The ENA images show how plasma is injected into the nightside magnetosphere as the interplanetary magnetic field (IMF) turns strongly southward. As the IMF B_z increases and the storm intensity decreases, the ENA images show that the ring current becomes closed and symmetric as IMF B_z reaches positive values.

Keywords: Ring current, geomagnetic storm, energetic neutral atom

1. Introduction

Geomagnetic storms are a global response of the magnetosphere of the Earth to solar wind conditions, an effect of enhanced magnetospheric electric field powered by reconnection in the dayside magnetopause during periods of southward interplanetry magnetic field (IMF). The southward IMF sets up a convection electric field from dawn to dusk over the magnetospheric tail which in turn convects both pre-existing and freshly supplied plasma towards Earth through $E \times B$ drift. As the plasma drifts closer to Earth, it is accelerated to higher energies and the effects of the curvature and gradient of the geomagnetic field become more significant such that the plasma begins to drift in more circular orbits around the Earth. As a result, positive ions above approximately 1 keV drift westward and electrons drift eastward around the Earth. When the convection electric field is weak (IMF $B_z \geq 0$) the plasma within ~ 7 R_E will drift on closed trajectories around the Earth. However, when the convection electric field is strong (IMF $B_z < 0$) plasma will drift on purely open trajectories from the nightside out through the dayside magnetopause.

Geomagnetic storms produce large scale effects on the geomagnetic field at the surface of the Earth. The increased energy density of plasma around the Earth generates a diamagnetic current density (carried mostly by the ions) that depresses the geomagnetic field according to Ampere's law. The average geomagnetic depression measured at observatories close to the equator is called the storm time disturbance (D_{st}) index which is commonly used to classify geomagnetic storms. The D_{st} can be taken as a preliminary measure of the current intensity. Since the current closes around the Earth as the IMF B_z increases to positive values, the current has been named the "ring current". A geomagnetic storm consists of a main phase when the ring current intensity increases rapidly due to a prolonged period of IMF B_z (Gonzalez and Tsurutani, 1987). The main phase lasts typically several hours. After the increase has stopped the storm enters the recovery phase where the ring current intensity slowly decays. This is related to the northward turning of the IMF and subsequent closing of the drift trajectories. The recovery phase lasts typically a couple of days. The exact cause of the main phase of geomagnetic storms and the loss mechanisms involved in the recovery phase are still controversial issues (Kamide et al., 1998).

Energetic netural atoms (ENA) are produced when energetic ($>> 1$ eV), singly charged ions charge exchange with the cold, neutral hydrogen exosphere around the Earth. The ions will be converted to ENAs and propagate unaffected by electric, magnetic and gravitational fields in straight lines from their production point. This allows space plasma to be remotely imaged by detecting the direction of the ENAs, much like the emissions of photons allows for optical imaging. The differential ENA flux (cm^2 sr s keV)$^{-1}$ detected can be described by the following line of sight (LOS) integral.

$$j_{ENA}(E) = \int_0^\infty j_{ION}(\ell) \sum_i \sigma_{10}^i(E)\, n_i(\ell)\, d\ell \qquad (1)$$

Here ℓ is the distance along a specific LOS, j_{ION} is the ion flux at each point along that LOS, σ_{10}^i is the charge exchange cross section between the ion of a given species and the exospheric neutral species i, and n_i is the exospheric number density of species i. The dominant ion species in the magnetosphere is hydrogen, but may also compete with oxygen. The probability for the "stripping" of the ENA en route to the spacecraft is negligible for ENAs emitted from the ring current.

Since the exospheric number density falls off exponentially with altitude, the ENA flux decreases with altitude although the parent ion flux does not necessarily need to do so. Therefore it is important to remember that ENA images do not directly represent the magnetospheric ion flux. To extract the ion flux one needs to simulate ENA images based on a model of the magnetospheric ion population (Roelof and Skinner, 2000; Perez et al., 2001). This will not be pursued in this report. However, keeping in mind the altitude variation of the exospheric number density, sufficient information from the ENA images alone can be extracted to conduct an analysis of the spatial and temporal dynamics of the plasma of the inner magnetosphere.

ENA imaging was first conceptualized by Roelof et al. (1985) and has today become an important tool for space plasma diagnostics. ENA images of the ring current have been obtained from some missions (Roelof, 1987; Henderson et al., 1997) using charged particle telescopes in the polar regions of the magnetosphere devoid of charged particles where the detectors therefore responded weakly to ENA. Dedicated ENA imagers have been carried by the Astrid satellite (Barabash, 1995; C:son Brandt et al., 1999), Cassini (Mitchell et al., 1998) and now IMAGE (Mitchell et al., 2000).

The IMAGE spacecraft was launched in March 2000 into a polar, elliptical orbit with an apogee altitude of 7.2 Earth radii (45,922 km/28,472 mi) (Burch, 2000). The location of the apogee will change during the course of the two-year mission, both in latitude and in local time. At the beginning of the mission, apogee was at approximately 40°north latitude and at dusk local time. As the Earth moves around the Sun, the plane of the orbit will shift relative to the Earth-Sun line (by 30°of longitude each month). For the data reported in this paper the orbit plane was approximately along the 1400-0200 magnetic local time (MLT) meridian and the magnetic latitude of apogee was about 50°. IMAGE carries three ENA imagers for three different energy ranges. It also carries one extreme ultraviolet (EUV) camera to image the plasmasphere, one far ultraviolet (FUV) camera to image the aurora, and one radio plasma imager (RPI) to sound plasma boundaries such as the plasmapause and the magnetopause.

This paper aims at giving a general overview of the response of the inner magnetosphere to the coronal mass ejection (CME) that swept over the Earth's magnetosphere on 15 July. Images taken in ENAs will be used to analyze the flow patterns of the ring current. The ENA images are obtained by the high energy neutral atom (HENA) imager on board IMAGE (Mitchell et al., 2000).

The IMAGE spacecraft received data throughout the storm; the FUV camera recorded auroral emissions filling the entire polar cap during the early phases of the shocked solar wind flow and the arrival of the CME. The HENA imager, although hampered by the background created by the intense solar energetic ion event, returned images in ENA showing the substorm activity on the night side, the early growth of the asymmetric ring current at storm main phase, and later the

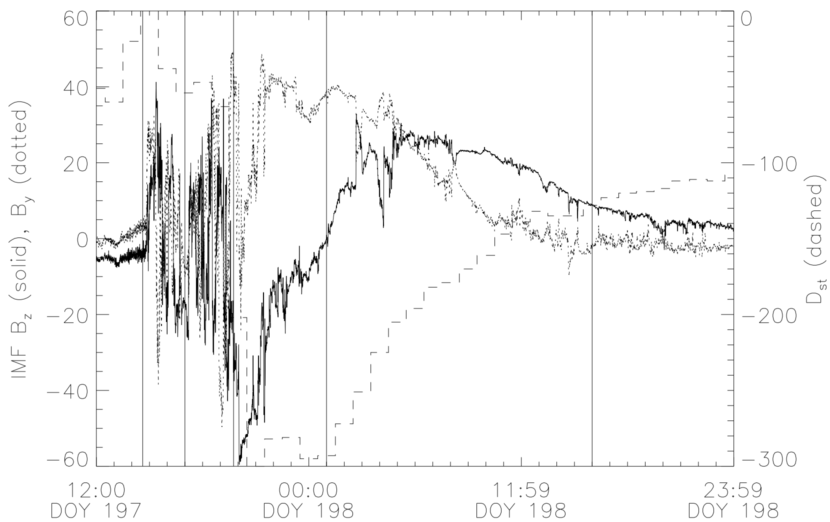

Figure 1. The z (solid) and y (dotted) component of the interplanetary magnetic field, and the D_{st} index (dashed).

decay of the symmetric ring current. About 50% of the storm main phase was not imaged by HENA, because that occurred while IMAGE passed through the radiation belts where the HENA instrument cannot operate. Although some of this data have been presented and discussed by Mitchell et al. (2001), several new aspects and results are included in this report.

In the next section we will give an overview of the geomagnetic storm and its effects on the geomagnetic environment caused by the arrival of the strongly southward IMF. In section 2.2 we will present and discuss in detail the main and recovery phase of the storm as seen by HENA. A brief summary is given in Section 3 at the end of the paper.

2. Observations

2.1. Overview of the storm

Late on July 15, 2000, a CME swept over the Earth's magnetosphere. This CME was associated with a solar flare that occurred a day before, producing high fluxes of energetic ions that continued to fill the space about Earth when the CME arrived. At 1437 UT, the shock wave ahead of the CME compressed the Earth's magnetosphere, pushing the subsolar magnetopause into geosynchronous orbit from its nominal position of about 10 R_E before the shock.

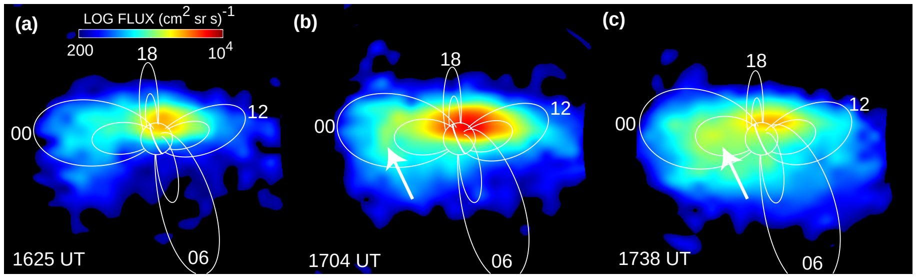

Figure 2. A substorm injection in the beginning of the main phase. ENA images at 39-50 keV (a) before the onset, (b) at onset, and (c) after dipolarization. Note how plasma has been brought closer to Earth, as shown by the arrows.

The compression of the dayside magnetosphere generated enhanced geomagnetic activity, as measured by the K_p index as well as by the AE index which responded to elevated substorm activity. Figure 1 shows the interplanetary magnetic field (IMF) B_z (solid line), IMF B_y (dotted line), and the D_{st} index (dashed line) for the day of year (DOY) 197 (15 July) and DOY 198 (16 July). The five vertical lines mark: 1437 UT, the arrival of the shock at Earth; 1700 UT, the substorm injection shown in Figure 2; 2000 UT the injection associated with the southward turning of IMF shown in Figure 3; 0100 UT (16 July) the early recovery shown in Figure 4; and 1647 UT (16 July) the late recovery shown in Figure 5. Although the IMF was compressed in the shock and the post-shock flow, its z-component was quite variable until about 1920 UT on July 15. At that time it went strongly negative, reaching a minimum value of -60 nT by about 2000 UT. This strong southward B_z, coupled with the high solar wind velocity, rapidly increased convection in the magnetosphere. Around 2200 UT, the IMF B_z at Earth became less negative (increasing to about -10 nT), before turning northward about an hour into July 16. This effectively ended the convective phase of the storm, and the ring current (as monitored by D_{st} index) began a steady decay during the third hour of the day.

2.2. IMAGE/HENA observations

2.2.1. *Main phase*

Up until 1437 UT on the 15 July, the IMF B_z was slightly negative and steady, and ENA images of the ring current display some nightside and dayside fluxes consistent with open drift trajectories where plasma flowed in from the nightside plasmasheet and out through the dayside magnetopause. After the shock related energetic ions dropped in intensity sufficiently for HENA to image above its background, the flow pattern did not change much until the first substorm (visible by

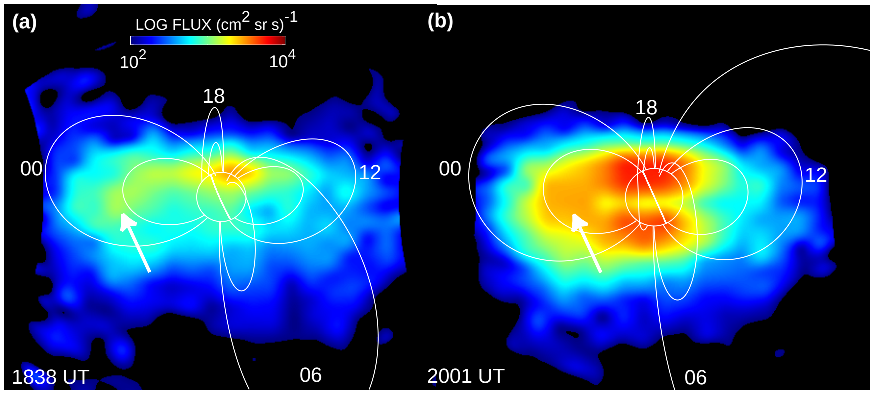

Figure 3. ENA images in the 39-50 keV range showing the enhanced convection leading to the main phase of the storm: (a) before main phase, and (b) at main phase enhancement with IMF B_z=-60 nT.

HENA) commenced at around 1700 UT as seen in Figure 2. All ENA images in this paper are displayed in an azimuthal projection with approximately 120°×120°field of view that resembles what the human eye would see. The dipole field lines for L=4 and L=8 are marked for reference at dawn, noon, dusk, and midnight. Figure 2a shows the ENA image at 1625 UT and displays weak ENA emissions on the nightside of the Earth outside L=4. More intense ENA emissions can be seen coming from close to the limb of the Earth. These are ENA emissions produced by nearly mirroring ions at low altitudes (∼500 km) where the exospheric O and N_2 start dominating (Roelof, 1997). The resulting ENA intensity can be 2-3 orders of magnitude brighter than the ENA emissions coming from higher altitudes where the ions only charge exchange with the much more tenous hydrogen geocorona. Hereafter we will refer to the ENA emissions coming from low altitudes and produced by charge exchange with O and N_2 as "low-altitude emissions". The low-altitude emissions will mainly show up when the line of sight (LOS) in a pixel cuts field lines at ∼500 km altitude at a pitch angle close to 90°. However, when the loss cone is filled due to sudden injections, brightening of the low-altitude emissions can be seen over a wider range of angles. The low-altitude emission can to some degree be considered as a point source, because the point-spread in the HENA instrument at the energies analyzed in this paper is typically 10°. The onset of the substorm has been identified using FUV images of the aurora. Enhanced ENA emissions from outside L=4 (arrow) as well as enhanced low-altitude emissions from enhanced preciptiation can be seen at the onset in Figure 2b. Enhanced precipitation is expected during onset both because the ions are initially energized in a thin field reversal region (current sheet) where their motion is effectively randomized by scattering in the sharply changing magnetic field structures, and because the very dynamic non-linear processes in the substorm current disruption region create waves which scatter the ions. This generates electric fields parallell to the geomagnetic field that accelerate ions towards the ionosphere. As the substorm onset proceeds, the stretched magnetic field in the magnetospheric tail dipolarizes and brings in plasma closer to the Earth, as can be seen at the arrow in Figure 2c. At this point the precipition of the ions (and the low-altitude ENA emissions) has decreased, as the magnetic field configuration is much more relaxed, and the wave generating dynamics have ceased to operate. The ENA intensity inside L=4 has increased a factor of two from Figure 2a to 2c.

As can be seen from Figure 1, the IMF B_z decreased between 1900 and 2000 UT, which we term the main phase of the storm. Figure 3a shows an ENA image from 1838 UT which is about 40 min before the large decrease of the IMF B_z down to -60 nT. The nightside ENA flux around L=4, marked by the arrow, and the lack of fluxes on the dayside and at dawn, indicate that plasma is being convected in from the tail and directly out through the dusk/noon magnetopause. As the IMF B_z goes rapidly down to -60 nT, the convection electric field enhances and plasma is being convected closer to the Earth, marked by the arrow in Figure 3b. However, another substorm occurred during the main phase, which energized plasma and brought it closer to the Earth. It is difficult at this stage to say how much of the injection was due to the substorm induced electric fields or due to the enhanced cross tail electric field.

The nightside ion flux increases due to the conservation of the adiabatic invariants as the plasma is convected into higher magnetic field strength. The flux is also intensified due to the energizations from sudden substorm induced electric field pulses. Both the strongly southward IMF and the lack of any ENA emissions from the dayside magnetosphere imply that the ring current ions are still on open drift trajectories in Figure 3b.

It is known that the abundance of O^+ ions competes with the abundance of protons in the ring current during large storms (Shelley et al., 1972; Hamilton et al., 1988; Daglis and Axford, 1996) and its energy density is often dominating that of the protons. The mass resolving capability of the HENA imager was unfortunately turned off during this storm so no species could be resolved. There is evidence that O^+ ions are extracted from the ionosphere in the mainphase of the larger storms. The O^+ enhancements are often associated with substorms (Daglis and Axford, 1996) and there are indications for direct injection and accelaration up to several keV from the auroral

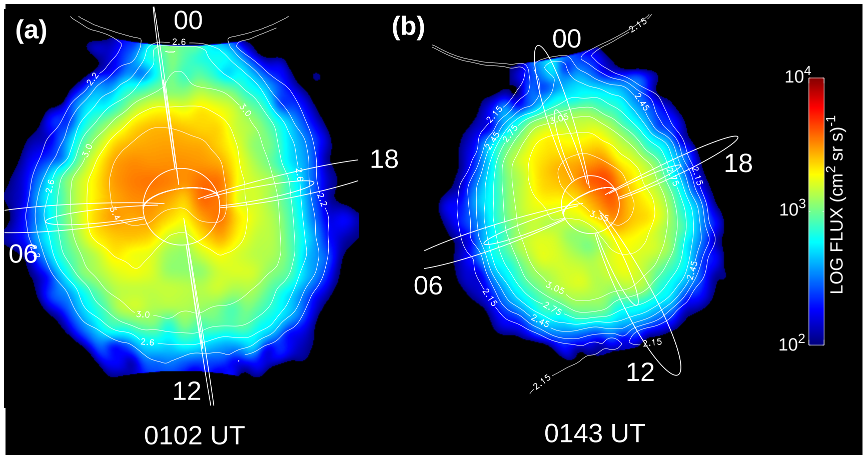

Figure 4. ENA images of the ring current at 39-50 keV during early recovery phase. Note the drift of the maximum from (a) to (b).

ionosphere (Möbius et al., 1987; Daglis et al., 1994). However, there are observations showing that the open polar cap is a significant source of O^+ (Pollock et al., 1990; Moore et al., 1997). Such a supply would transport O^+ ions further down the geomagnetic tail which raises the question of how the ions got transported back in to the near Earth magnetosphere where they have been observed. Therefore it is of high priority to pursue composition analysis of the HENA images of other storms than this one. This is currently being undertaken by the HENA team and we hope to be able to report on these results soon.

2.2.2. *Recovery phase*

On 16 July at 0102 UT IMAGE came back up over the north pole. From Figure 4a we see that the ring current displayed a minimum around noon. Contours have been added to aid the eye. The intense ENA emissions from the surface of the Earth around dusk are low-altitude emissions from enhanced ion precipitation, but the intense emissions from the dawn side come from a maximum in the ring current ion flux. At this point the IMF B_z was slightly negative and climbing towards 0 nT (see Figure 1), which means that the magnetospheric convection was weakening and the ring current was almost closed. During this stage of the storm the losses include convection out through the magnetopause and charge exhcange with the geocorona. This has recently been modeled by Liemohn et al. (1999) and Liemohn et al. (2001). The maximum on the dawnside is due to the strongly positive IMF B_y ($\sim$+40 nT) which effectively skews the local time pattern of the electric potential in the equatorial magnetosphere (Khurana et al., 1996) so that the electric

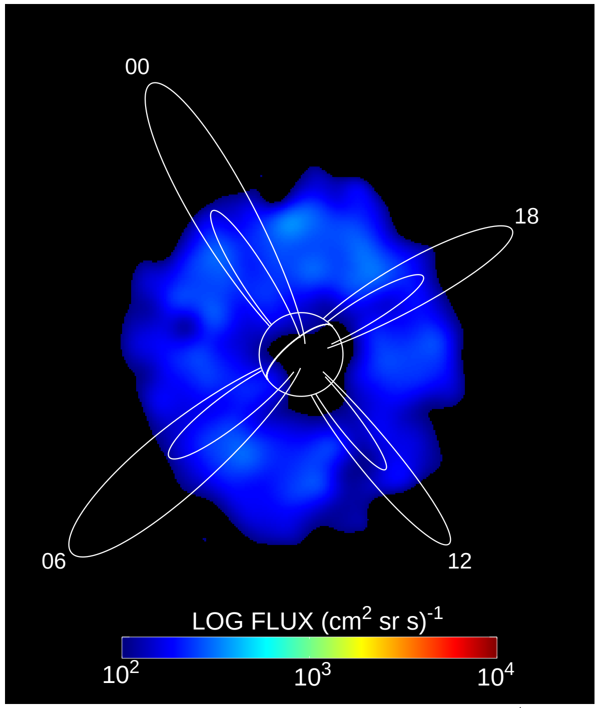

Figure 5. The ring current at 39-50 keV on 16 July 1647 UT (late recovery). Note that the ring current is closed.

potential minimum is rotated towards dawn. This results in maximum energization in this region and therefore also higher differential ion flux and explains the preference of higher ENA flux towards dawn in Figure 4a. As IMF B_z reaches +10 nT the magnetospheric convection is practically turned off and the ion population in the maximum becomes trapped and starts gradient-curvature drift in a westward sense. This displacement can be seen in Figure 4b. The ring current closed entirely sometime after 16 July 0200 UT. Figure 5 shows an ENA image taken on 16 July 1647 UT in the same 39-50 keV range. This figure is shown in the same scale and energy range as Figure 4 and we can see that the overall ENA flux has decreased significantly and that the ring current is symmetric and closed. During this stage of the recovery the main loss mechanism of the ring current is through charge exchange with the geocorona.

3. Summary and conclusions

We have discussed the effects of the Bastille day storm on the magnetosphere and especially the ring current. We presented global ENA observations in the 39-50 keV range of the ring current. Shortly after the CME shock arrived at Earth, a substorm at 1700 UT was observed to inject plasma in to around L=4. The beginning of the main phase was marked by the intense decrease of IMF B_z down to -60 nT. This, together with a substorm around 1900 UT, injected and energized more plasma in the nightside magnetosphere. Plasma during this time was flowing from the nightside and out through the dayside magnetopause with little or no trapping. As the IMF B_Z increased to less negative values, the convection of plasma from the nightside to the dayside magnetosphere decreased and the ring current started to close and decay in strength. The primary loss processes during the first stage of the recovery were therefore convective loss through the dayside magnetopause as well as charge exchange. In the later stages of the recovery the ring current was symmetric and closed and the main loss process was therefore charge exchange with the neutral hydrogen geocorona. The evolution of the ring current ion population was as follows.

1. The main phase of the storm begins when the ring current intensity is enhanced through convection set up by the arrival of the strongly southward IMF component (-60 nT) and high solar wind velocity.

2. At the maximum ring current intensity, as measured by the D_{st} index, the convection is also at its maximum allowing plasma to escape through the dayside magnetopause.

3. As the negative values of IMF B_z tend towards zero the ring current intensity decreases.

4. The IMF B_z is still negative in the early stage of storm recovery and the ring current displays a local-time asymmetry, which means that some plasma could still drift on open trajectories and be lost through the dayside magnetopause. Therefore the losses during this stage was charge exchange and drift out through the dayside magnetopause.

5. As the IMF B_z reaches positive values the ring current becomes symmetric and closed. The main loss mechanism in this phase is therefore only charge exchange.

Acknowledgements

References

Barabash, S.: 1995, 'Satellite Observations of the Plasma-Neutral Coupling Near Mars and the Earth'. Ph.D. thesis, Swed. Inst. of Space Phys., Kiruna.

Burch, J. L. (ed.): 2000, *The IMAGE mission*. Kluwer Academic. Reprinted from *Space Sci. Rev.*, vol. 91, Nos. 1-2, 2000.

C:son Brandt, P., S. Barabash, O. Norberg, R. Lundin, E. C. Roelof, and C. J. Chase: 1999, 'ENA Imaging at Low Altitudes From the Swedish Micro Satellite Astrid: Images and Spectral Analysis'. *J. Geophys. Res.* **104**(A2), 2367–2379.

Daglis, I. A. and W. I. Axford: 1996, 'Fast ionospheric Response to Enhanced Activity in Geospace: Ion Feeding of the Inner Magnetotail'. *J. Geophys. Res.* **101**(A3), 5047–5065.

Daglis, I. A., S. Livi, E. T. Sarris, and B. Wilken: 1994, 'Energy density of ionospheric and solar wind origin ions in the near-Earth magnetotail during substorms'. *J. Geophys. Res.* **99**, 5691–5703.

Gonzalez, W. D. and B. T. Tsurutani: 1987, 'Criteria of interplanetary parameters causing intense magnetic storms (D_{st} <-100 nT)'. *Planetary and Space Sci.* **35**, 1101.

Hamilton, D. C., G. Gloeckler, F. M. Ipavich, W. Studemann, B. WIlken, and G. Kremser: 1988, 'Ring current development during the great geomagnetic storm of February 1986'. *J. Geophys. Res.* **93**(A12), 14343–14355.

Henderson, M. G., G. D. Reeves, H. E. Spence, R. B. Sheldon, A. M. Jorgensen, J. B. Blake, and J. F. Fennell: 1997, 'First Energetic Neutral Atom Images from Polar'. *Geophys. Res. Lett.* **24**, 1167–1170.

Kamide, Y., W. Baumjohann, I. A. Daglis, W. D. Gonzalez, M. Grande, J. A. Joselyn, R. L. McPherron, J. L. Phillips, E. G. D. Reeves, G. Rostoker, A. S. Sharma, H. J. Singer, B. T. Tsurutani, and V. M. Vasyliunas: 1998, 'Current understanding of magnetic storms: Storm-substorm relationships'. *J. Geophys. Res.* **103**(A8), 17705–17728.

Khurana, K. K., R. J. Walker, and T. Ogino: 1996, 'Magnetospheric convection in the presence of interplanetary magnetic field B_y: A conceptual model and simulations'. *J. Geophys. Res.* **101**(A3), 4907–4916.

Liemohn, M. W., J. U. Kozyra, V. K. Jordanova, G. V. Khazanov, M. F. Thomsen, and T. E. Cayton: 1999, 'Analysis of the early phase ring current recovery mechanism during geomagnetic storms'. *Geophys. Res. Lett.* **25**, 2845–2848.

Liemohn, M. W., J. U. Kozyra, M. F. Thomsen, J. L. Roeder, G. Lu, J. E. Borovsky, and T. E. Cayton: 2001, 'The dominant role of the asymmetric ring current in producing the stormtime *Dst*'. *J. Geophys. Res.* in press.

Mitchell, D. G., K. C. Hsieh, C. C. Curtis, D. C. Hamilton, H. D. Voss, E. C. Roelof, and P. C:son Brandt: 2001, 'Imaging two geomagnetic storms in energetic neutral atoms'. *Geophys. Res. Lett.* in press.

Mitchell, D. G., S. E. Jaskulek, C. E. Schlemm, E. P. Keath, R. E. Thompson, B. E. Tossman, J. D. Boldt, J. R. H. abd G. B. Andrews, N. Paschalidis, D. C. Hamilton, R. A. Lundgren, E. O. Tums, P. Wilson IV, H. D. Voss, D. Prentice, K. C. Hsieh, C. C. Curtis, and F. R. Powell: 2000, 'High energy neutral atom (HENA) imager for the IMAGE mission'. *Space Sci. Rev.* **91**, 67–112.

Mitchell, D. G., S. M. Krimigis, A. F. Cheng, S. E. Jaskulek, E. P. Keath, B. H. Mauk, R. W. McEntire, E. C. Roelof, C. E. Schlemm, B. E. Tossman, and D. J.

Williams: 1998, *The imaging neutral camera for the Cassini mission to Saturn and Titan*, Vol. 103 of *Geophysical Monograph*. Washington, DC: AGU.

Möbius, E., M. Scholer, B. Klecker, D. Hovestadt, G. Glockler, and F. M. Ipavich: 1987, 'Acceleration of ions of ionospheric origin in the plasma sheet during substorm activity'. In: A. T. Y. Lui (ed.): *Magnetotail physics*. Baltimore, MD: Johns Hopkins Univ. Press, pp. 231–234.

Moore, T. E., C. R. Chappell, M. O. Chandler, P. D. Craven, B. L. G. C. J. Pollock, D. T. Young, J. H. Waite Jr., J. E. Nordholt, M. F. Thomsen, D. J. McComas, J. J. Berthelier, W. S. Williamson, R. Robson, and F. S. Mozer: 1997, 'High-altitude observations of the polar wind'. *Science* **277**, 349.

Perez, J. D., G. Kozlowski, P. C. Brandt, D. G. MItchell, J. M. Jahn, C. J. Pollock, and X. Zhang: 2001, 'Initial ion equatorial pitch angle distributions from energetic netural atom images obtained by IMAGE'. *Geophys. Res. Lett.* in press.

Pollock, C. J., M. O. Chandler, T. E. Moore, J. H. Waite Jr., C. R. Chappell, and D. A. Gurnett: 1990, 'A survey of upwelling ion event characteristics'. *J. Geophys. Res.* **95**, 18969–18980.

Roelof, E. C.: 1987, 'Energetic Neutral Atom Image of a Storm-Time Ring Current'. *Geophys. Res. Lett.* **14**, 652–655.

Roelof, E. C.: 1997, 'ENA Emissions from Nearly Mirroring Magnetospheric Ions Interacting with the Exobase'. *Adv. Space Res.* **20, (3)**, 361–366.

Roelof, E. C., D. G. Mitchell, and D. J. Williams: 1985, 'Energetic Neutral Atoms (E≈50 keV) from the Ring Current: IMP 7/8 and ISEE 1'. *J. Geophys. Res.* **90**(A11), 10991–11008.

Roelof, E. C. and A. J. Skinner: 2000, 'Extraction of Ion Distributions from Magnetospheric ENA and EUV Images'. *Space Sci. Rev.* **91**, 437–459.

Shelley, E. G., R. G. Johnson, and R. D. Sharp: 1972, 'Satellite Observations of Energetic Heavy Ions during a Geomagnetic Storm'. *J. Geophys. Res.* **77**(31), 6104–6110.